Geochemical evidence for enhanced fluid flux due to overlapping subducting plates

HITOMI NAKAMURA[1*†], HIKARU IWAMORI[2] AND JUN-ICHI KIMURA[3‡]

[1]Department of Geosystem Engineering, University of Tokyo, Hongo, Tokyo 113-0033, Japan
[2]Department of Earth and Planetary Science, University of Tokyo, Hongo, Tokyo 113-0033, Japan
[3]Department of Geoscience, Shimane University, Matsue city, 690-8504, Japan
*Present address: Institute of Geoscience and Geoinformation, Geological Survey of Japan (AIST), Tsukuba, Ibaraki, 305-8567, Japan
‡Present address: Institute for Research on Earth Evolution (IFREE), Japan Agency for Marine-Earth Science and Technology (JAMSTEC), Yokosuka 237-0061, Japan
†e-mail: hitomi-nakamura@aist.go.jp

Published online: 11 May 2008; doi:10.1038/ngeo200

Aqueous fluids released from subducting plates play an important role in magma generation in many arc settings[1–4]. However, different hypotheses have been proposed for the origin of these fluids, the extent to which they mix with the mantle wedge and spatial variations in their composition[2–4], especially at complex settings involving more than one subducting plate. Central Japan is one such setting, where the Pacific and Philippine Sea plates subduct underneath the North American and Eurasian plates and cause extensive arc magmatism to the west and north of Tokyo. Here, we use geochemical data for rocks from 28 Quaternary volcanoes in central Japan to quantify the relative contribution of fluids originating from the two subducting plates and their spatial distribution. We find that the fluid originating from the Philippine Sea plate is chemically distinct and its flux is localized, as compared with the larger-scale flux from the Pacific plate. In the regions where these two plates overlap, the Philippine Sea plate does not seem to significantly inhibit fluid flow from the Pacific plate below; instead, this geometry leads to enhanced fluid flux. Regional variations in fluid flux and composition are controlled primarily by the geometry and configuration of the subducting plates.

Beneath central Japan, the Philippine Sea plate (PHS) subducting from the southeast overlaps with the Pacific plate (PAC) subducting from the east (Fig. 1). This overlap could produce more fluid from the two slabs and cause extensive magmatism with stronger fluid signatures, compared with arc magmatism with a single subducting slab. To test this possibility, we have carried out regional field and geochemical surveys, and have found systematic spatial variations in the Pb–Sr–Nd isotopic ratios for 46 samples from 28 Quaternary volcanoes in central Japan (Fig. 2 and Supplementary Information, Table S1), which were chosen to cover the whole area and the compositional range from basaltic to andesitic rocks in each volcano. The lavas in the central region (north of the Izu peninsula, ranging from the Fuji to the Myoko volcano) are distinctly depleted in radiogenic components, compared with those in the eastern and western regions.

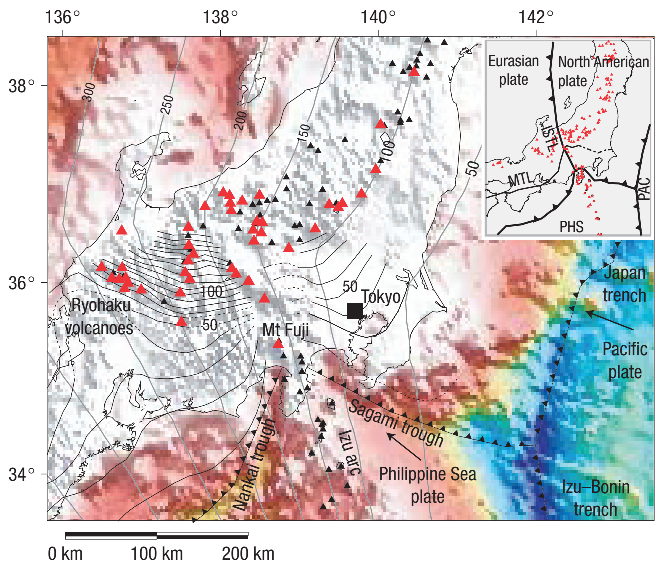

Figure 1 Tectonic setting and sample localities in central Japan. The PAC subducts beneath central Japan from east-southeast at 7–9 cm yr^{-1}, whereas the PHS subducts from the southeast at 3–5 cm yr^{-1}. The depth contours of the upper surface of the subducted slabs are shown for the PAC at 50 km intervals (grey solid lines) and the PHS at 10 km intervals (black solid lines, or dashed lines where it is not well resolved)[17–20]. The inset shows the plate boundaries (thick lines) and other major tectonic boundaries, the Itoigawa–Shizuoka Tectonic Line (ISTL) and the Median Tectonic Line (MTL) (thin solid lines or dashed lines where they are not exposed at the surface or are unclear).

In the adjacent Izu and northeast Japan arcs, systematic spatial variations are also reported[2–4]. In the northern part of the Izu arc, the compositions of rocks from the volcanic front with low Nb/Pb to the back-arc region with high Nb/Pb show a clear single trend in the $^{207}Pb/^{204}Pb$–Nb/Pb diagram (Fig. 3a), which can be explained by mixing between the depleted mid-ocean-ridge-basalt mantle[5] (DMM) and fluid with $^{207}Pb/^{204}Pb \sim 15.56$ and Nb/Pb ~ 0 (ref. 3). Fluid with a similar composition was found in northeast Japan[4], which indicates that the $^{207}Pb/^{204}Pb$ ratio of the aqueous fluid released from the subducting PAC (hereafter referred to as PAC fluid) is relatively uniform (15.56 ± 0.016) (refs 2–4) over a wide area from the Izu arc to the northeast Japan arc. This PAC fluid is also released beneath central Japan: the compositions of rocks in the central region (the most depleted area in Fig. 2) lie along a

© 2008 Nature Publishing Group

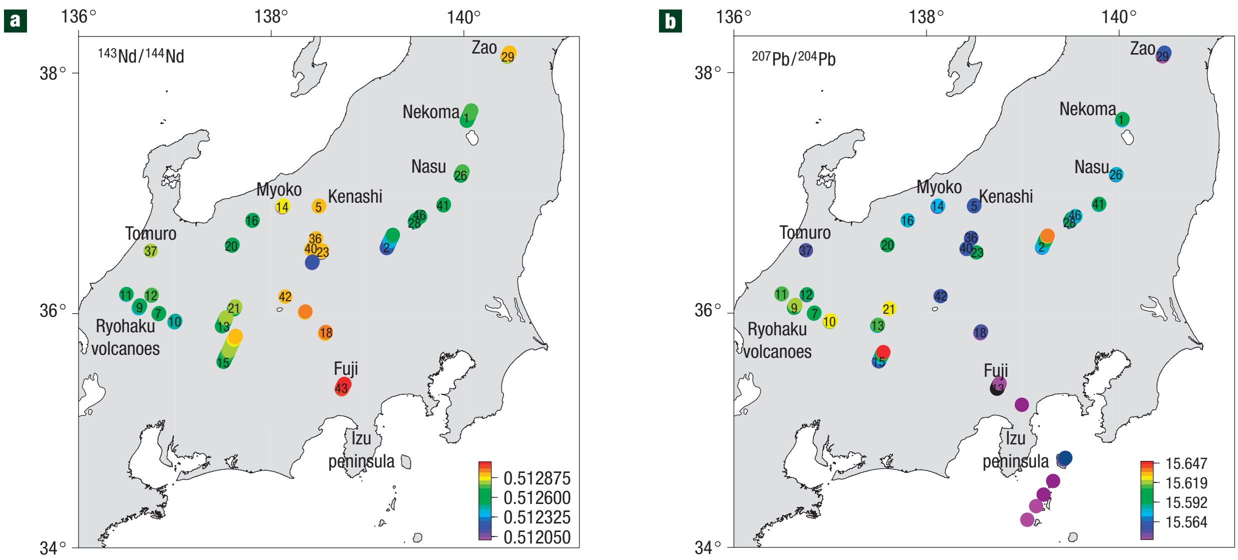

Figure 2 Spatial variations of $^{143}Nd/^{144}Nd$ and $^{207}Pb/^{204}Pb$ of the Quaternary volcanic rocks in central Japan. The rocks with silica contents of less than 65 wt% have been selected. **a**, $^{143}Nd/^{144}Nd$. **b**, $^{207}Pb/^{204}Pb$. The number attached to each volcano indicates the ID number (#), and the corresponding compositional data are listed in Supplementary Information, Tables S1,S2. The following data are compiled from previous studies[3,25,27–29]: Akagi (#2), Nantai (#28), Nasu (#26), Nyoho (#46), Nekoma (#1) volcanoes, the Ueno basalts (#15) and basalts in the northern part of the Izu arc. In each volcano, the isotopic variation is shown by the corresponding colour variation within each column.

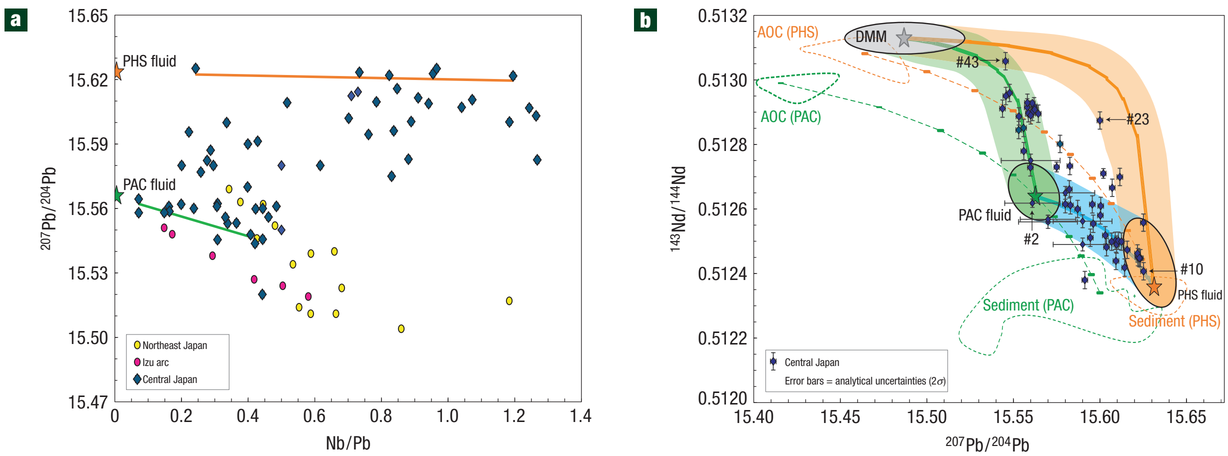

Figure 3 The Nb/Pb versus $^{207}Pb/^{204}Pb$ and $^{207}Pb/^{204}Pb$ versus $^{143}Nd/^{144}Nd$ diagrams of volcanic rocks. a, Comparison between central Japan (see Supplementary Information, Table S1 and previous studies[25,27–29]), Izu[3] and northeast Japan[4]. Regression lines for the central region (green line) and Ryohaku volcanoes (orange line) in central Japan correspond to mixing between PAC fluid or PHS fluid and average DMM (ref. 5). **b**, Mixing relationship for PAC fluid, PHS fluid and average DMM, with the compositions of sediment and AOC from the PAC (refs 8,9) and PHS (refs 10,11). The dashed curves represent mixing between the average sediment fluid and AOC fluid, marked off every 10 wt%. Thick solid lines represent mixing between PAC fluid, PHS fluid and average DMM (ref. 5), whereas ellipsoids and transparent bands connecting the ellipsoids represent the uncertainties ($\pm 1\sigma$) of the three endmembers and their mixing.

mixing line between DMM and PAC fluid ($^{207}Pb/^{204}Pb = 15.562$ and $Nb/Pb = 0$). To explain the compositions of volcanic rocks in the eastern and western regions, at least one other endmember with a high $^{207}Pb/^{204}Pb$ ratio at $Nb/Pb \sim 0$ is required (Fig. 3a). Within the higher $^{207}Pb/^{204}Pb$ range, the compositions of the Ryohaku volcanoes located in the western region show a clear trend extending from DMM, and give the intercept as a composition of another endmember ($^{207}Pb/^{204}Pb = 15.628$ and $Nb/Pb = 0$). Model calculations to test mass balance using several candidates for the endmember (for example, aqueous fluid or melt derived from subducted sediment or altered oceanic basaltic crust, hereafter referred to as AOC), as well as constraints from thermal modelling showing a very cold geotherm beneath central Japan due to overlapping plates[6,7], suggest that this endmember is likely to be an aqueous fluid derived from the subducted slab (see the Methods section and Supplementary Information, Fig. S1b). Considering

© 2008 Nature Publishing Group

that the subducted PHS is clearly observed beneath the Ryohaku volcanoes (Fig. 1), we deduce that the fluid is derived from the subducted PHS (hereafter referred to as PHS fluid, see also Supplementary Information, Methods).

In addition to the $^{207}Pb/^{204}Pb$ ratio, $^{143}Nd/^{144}Nd$, $^{87}Sr/^{86}Sr$, $^{206}Pb/^{204}Pb$, $^{208}Pb/^{204}Pb$ and trace-element abundances of PAC fluid and PHS fluid are estimated as follows. Using reported compositions of subducting sediments and AOC (refs 8–11), which are the two major sources of fluid from subducting slabs, and mobilities of elements during dehydration[12–14], we can calculate the compositions of fluids derived from sediments (hereafter referred to as sediment fluid) and AOC (referred to as AOC fluid) during the dehydration processes of the subducting PAC and PHS, respectively. The dehydration process of the PAC beneath central Japan is well constrained by numerical simulations[7], in which the depth range of major dehydration (150–300 km) is greater than that of the adjacent northeast Japan and Izu arcs owing to the cold geotherm associated with overlapping subduction. Although there is no direct quantitative model for the dehydration of the subducting PHS, we can reasonably estimate the dehydration processes on the basis of the predicted thermal structures[6,7]. These results, together with studies on shallow dehydration processes[15], indicate that most of the H_2O contained initially in the subducted sediment and AOC is released from the slab to form a thin serpentinite layer just above the slab[6,7,16]. This serpentinite dehydrates at 150–300 km depths for the PAC and 90–150 km depths for the PHS (refs 6,7). These constraints on the multistage dehydration processes enable us to calculate (1) the compositions of sediment fluid and AOC fluid for the PAC and PHS, respectively, and (2) the compositions of PAC fluid and PHS fluid integrating the respective sediment fluid and AOC fluid, on the basis of the $^{207}Pb/^{204}Pb$ constraint obtained in Fig. 3a (see Supplementary Information, Methods for the details).

Mixing of the estimated PAC fluid, PHS fluid and DMM, which leads to a fluid-fluxed mantle wedge as the source region of magmas, explains the compositional variation of volcanic rocks in the Pb–Nd isotopic system (Fig. 3b) using two parameters, R_{fluid} (weight proportion of the fluid added to the mantle of the melting region, whose unit is hereafter given as 'kg fluid/kg mantle') and α_{PHS} (= PHS fluid/(PAC fluid + PHS fluid) in weight ratio). The spatial distributions of R_{fluid} and α_{PHS} are shown in Fig. 4. On the basis of the average values of R_{fluid} and α_{PHS}, the studied region can be divided into three areas from east to west: the Nasu area with relatively large R_{fluid} (0.016 kg fluid/kg mantle) and intermediate to small α_{PHS} (0.21) values, the Fuji–Myoko area with small R_{fluid} (0.004 kg fluid/kg mantle) and small α_{PHS} (0.14) values and the Ryohaku area with large R_{fluid} (0.020 kg fluid/kg mantle) and large α_{PHS} (0.50) values. A significant amount of PAC fluid is included in the Nasu and Ryohaku areas (0.010 kg PAC fluid/kg mantle on average). Even in the Fuji–Myoko area, where R_{fluid} is distinctly small compared with that in the Nasu and Ryohaku areas, an appreciable amount of PAC fluid is involved (0.003 kg PAC fluid/kg mantle). These results suggest that, although the PHS slab exists beneath the Fuji–Myoko and Ryohaku areas[17–20], it does not shut off the fluid flux from the underlying PAC slab. In contrast, the contribution of PHS fluid differs markedly between the three areas: moderately large amounts in the Nasu area (0.002–0.004 kg PHS fluid/kg mantle), almost negligible amounts in the Fuji–Myoko area (0.000–0.001 kg PHS fluid/kg mantle) and large amounts beneath the Ryohaku volcanoes in the southern part of the Ryohaku area (0.012–0.036 kg PHS fluid/kg mantle), which decreases northward (for example, 0.000 kg PHS fluid/kg mantle for the Tomuro volcano). The regional features indicate that combination of the regional input of PAC fluid and the local input of PHS fluid enhances the overall fluid flux in central Japan: the estimated R_{fluid} (0.001–0.040 kg fluid/kg mantle) is significantly larger than that of the Izu arc (~0.002–0.010 kg fluid/kg mantle)[3] owing to the overlapping subduction.

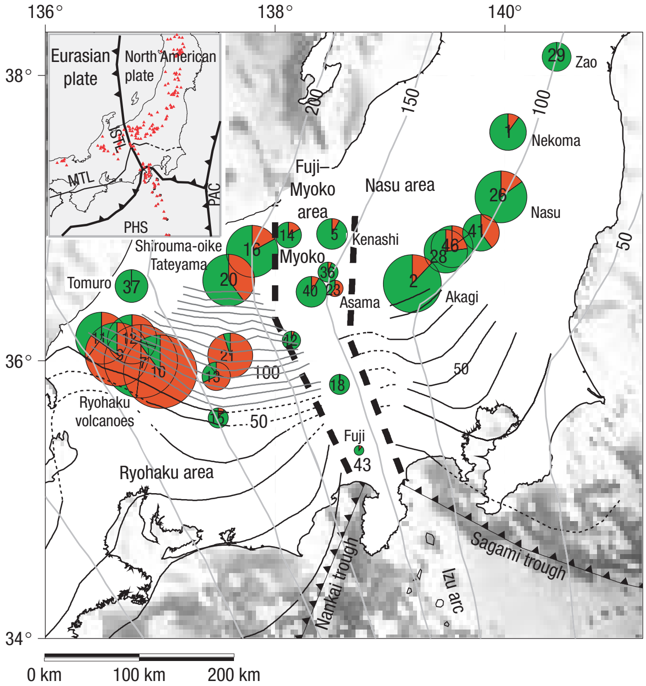

Figure 4 Spatial distribution of fluid flux from the PAC and PHS slabs. The radius of each circle is proportional to R_{fluid}. The areal proportion of the orange part (PHS fluid) corresponds to α_{PHS}, whereas the green part represents the proportion of PAC fluid. Thick dashed lines represent the boundaries between the Nasu, Fuji–Myoko and Ryohaku areas on the basis of the spatial distribution of R_{fluid} and α_{PHS}. The boundary between the Fuji–Myoko and Ryohaku areas almost coincides with the ISTL in the inset. The average uncertainties are estimated to be ±0.005 (kg fluid/kg mantle) for R_{fluid} and ±0.1 for α_{PHS}, on the basis of Fig. 3b. Depth contours for subducted plates are as in Fig. 1.

The geochemical segmentation described above correlates well with the configuration of the subducted PAC and PHS slabs (Fig. 4), which has been determined by the distribution of hypocentres, analyses of converted waves and tomographic studies[17–20]. In the Nasu area, the volcanoes are aligned ~100 km above the upper surface of the subducted PAC slab[17] as an extension of the volcanic front from the north, where input of PAC fluid is expected through a dehydration process similar to that beneath the northeast Japan arc[21]. The volcanoes in the Nasu area are also located ~90 km above the leading edge of the seismic PHS slab subducted from the south[21]. Because the leading edge is heated to 700 °C at 2.5 GPa with the corner flow induced by subduction of the PAC (ref. 7), the PHS slab can supply a relatively small amount of fluid[6,22] around the leading edge. This combination of PAC fluid and a smaller amount of PHS fluid may explain the observed R_{fluid} and α_{PHS} values in the Nasu area.

In the Fuji–Myoko area, the volcanoes are aligned 150–200 km above the subducted PAC slab[17], where only a small supply of PAC fluid is predicted as major dehydration occurs at greater depth (200–300 km) owing to the low geothermal gradient associated with overlapping subduction[7]. In the northern part, the lack of overlapping subduction (Fig. 4) shifts the dehydration reaction to shallower depths (150–250 km), exhibiting a transition to the adjacent northeast Japan arc. This causes the larger contribution of PAC fluid in the northern part (for example, the Kenashi volcano

© 2008 Nature Publishing Group

in the Fuji–Myoko area, and the Shirouma-oike and Tateyama volcanoes in the Ryohaku area, Fig. 4). On the other hand, the subducted PHS slab is observed beneath the southern part as an aseismic slab[18–20], which is thought to be the former Izu arc (Fig. 1) consisting of relatively anhydrous rocks[23], without a clear Wadati–Benioff plane (Fig. 4). The dry condition of the PHS subducted beneath the Fuji–Myoko area and a small subduction velocity due to the Izu–Honshu collision probably contribute to less enbrittlement[24] and the aseismic nature. These distinct features are consistent with the observed small R_{fluid} and α_{PHS} values in the Fuji–Myoko area.

In the Ryohaku area, the volcanoes are located ~200–300 km above the subducted PAC slab[17], where major dehydration of serpentinite just above the slab occurs at this anomalously deep range, owing to the very low geothermal gradient associated with the overlapping subduction[7]. The expelled PAC fluid is observed over the Ryohaku area, even in the central part where the PHS slab clearly overlaps (Fig. 4), again suggesting that the PHS slab does not shut off the PAC fluid flux. In addition, the PHS slab steeply dips beneath a narrow zone around 36° N (ref. 17) (Fig. 4), which may cause a concentrated upward flux of PHS fluid, corresponding to the Ryohaku volcanoes with large α_{PHS}. The PHS slab does not reach the northern Ryohaku area (north of ~36.5° N) (ref. 17), so there is no contribution of PHS fluid in the north (Tomuro volcano).

This coincidence between the geochemical and seismic features indicates that the geometry and configuration of the subducted PHS primarily control the distribution of PHS fluid. The input from the subducted PHS slab almost disappears around the Nekoma volcano ($\alpha_{\text{PHS}} = 0.10$) towards the ordinary northeast Japan arc (for example, $\alpha_{\text{PHS}} = 0.00$ at the Zao volcano[25], Fig. 4), whereas it disappears around the Fuji volcano ($\alpha_{\text{PHS}} = 0.10$) towards the Izu arc. Although the precise locations are not well constrained owing to the uncertainties involved in α_{PHS}, the transition reflects the spatial extent of the subducted PHS slab (Fig. 4). These results suggest that the geochemical variations of arc volcanic rocks can be a direct indicator of the extent of subducted slab. Therefore, the geochemical approach could be useful to map the subducted slabs in other arcs where the configuration of slabs is complicated or the geometry is obscure owing to low seismicity (for example, part of the Luzon arc[26]), like in central Japan.

METHODS

The dehydration processes of the subducted PAC and PHS slabs are described in detail in the Supplementary Information. The trace-element and isotopic compositions of sediment fluid and AOC fluid, together with those of the resultant PAC fluid and PHS fluid, are calculated on the basis of those of sediment and AOC sampled from the sea floors before subduction[8–11] and the mobilities of the elements[12–14] during a series of multistage dehydration processes[6,7] (see Supplementary Information, Methods). As a consequence, the compositions of PAC fluid and PHS fluid can be approximately broken down into sediment fluid and AOC fluid components. The sediment fluid/AOC fluid ratios are estimated to be 30:70 for PAC fluid and 97:3 for PHS fluid, on the basis of the ^{207}Pb/^{204}Pb constraint obtained in Fig. 3a.

As both the PAC and PHS slabs beneath central Japan are not young (~130 Myr and >40 Myr old, respectively) in the cold environment due to overlapping subduction[7], melting of the two slabs is likely to be inhibited[6]. Seismic tomography beneath the area[17] also does not show any clear evidence for slab melting. In terms of mass balance, mixing between aqueous fluids derived from the PAC and PHS slabs and DMM explains the observed isotopic and trace-element compositions (Fig. 3 and Supplementary Information, Figs S1,S2), which justifies the use of elemental partitioning or mobility between aqueous fluids and minerals for estimation of the dehydration processes. Nevertheless, the possibility of slab melting and its contribution to PHS fluid cannot be entirely ruled out, because some of the data with high ^{207}Pb/^{204}Pb and Nd/Pb ratios may also be explained by the involvement of such a melt component, especially a sediment-derived melt (see Supplementary Information, Fig. S1b). It should be noted that even if such a sediment-derived melt is involved in PHS fluid, isotopic systematics and the mixing model for PAC fluid, PHS fluid and DMM are robust because they are mostly constrained by the isotopic ratios, although the mixing curves and the mixing proportions are slightly modified.

The Supplementary Information shows all of the compositional data used in this study (see Supplementary Information, Table S1). The estimated R_{fluid} and α_{PHS} values shown in Fig. 4 are listed in Supplementary Information, Table S2, which are calculated on the basis of the mixing model in the ^{207}Pb/^{204}Pb–^{143}Nd/^{144}Nd system (Fig. 3b), as the Pb–Nd isotopic systematics provides the best resolution for quantifying R_{fluid} and α_{PHS}. We also present the other systematics involving all of the isotopic ratios (^{206}Pb/^{204}Pb, ^{207}Pb/^{204}Pb, ^{208}Pb/^{204}Pb, ^{87}Sr/^{86}Sr, ^{143}Nd/^{144}Nd) and the Nd/Pb ratio (see Supplementary Information, Figs S1,S2), which are consistent with the mixing model shown in Fig. 3b. The four volcanoes (#2, #10, #23, #43) that represent the regional compositional variations are shown in Fig. 3b, Supplementary Information, Figs S1a,S2 to demonstrate the consistency between the different systems. In addition, the Sr isotopic ratios calculated from R_{fluid} and α_{PHS} that are based on the independent ^{207}Pb/^{204}Pb–^{143}Nd/^{144}Nd systematics are listed in Supplementary Information, Table S2 to quantitatively confirm the consistency.

The average uncertainties for R_{fluid} and α_{PHS} are estimated to be ± 0.005 (kg fluid/kg mantle) and ± 0.1, respectively, which arise from uncertainties in the ^{207}Pb/^{204}Pb ratio of the two fluids (± 0.016) evaluated in Fig. 3a and the variability of the average compositions of subducted materials for each plate and DMM in Fig. 3b (for PAC, ^{207}Pb/^{204}Pb = 15.600 (15.524–15.64), ^{143}Nd/^{144}Nd = 0.51234 (0.512175–0.512456) in sediment[8] and ^{207}Pb/^{204}Pb = 15.4224 (15.406–15.452), ^{143}Nd/^{144}Nd = 0.51299 (0.512944–0.513012) in AOC (ref. 9); for PHS, ^{207}Pb/^{204}Pb = 15.629(15.609–15.648), ^{143}Nd/^{144}Nd = 0.51233 (0.512325–0.512386) in sediment[10] and ^{207}Pb/^{204}Pb = 15.629 (15.437–15.496), ^{143}Nd/^{144}Nd = 0.51310 (0.513003–0.513117) in AOC (ref. 11); for DMM (ref. 5), ^{207}Pb/^{204}Pb = 15.486 ± 0.039, ^{143}Nd/^{144}Nd = 0.51313 ± 0.00005). However, the uncertainties shift R_{fluid} and α_{PHS} uniformly for all of the observed data in Fig. 3b, without significantly modifying the relative compositional relationships between the volcanoes. As a consequence, the regional variations in R_{fluid} and α_{PHS} are robust against these uncertainties in terms of the distinct characteristics between the Nasu, Fuji–Myoko and Ryohaku areas.

It should also be noted that the isotopic ratios of the rocks in central Japan are almost independent of the silica content and nearly constant for each volcano (see Supplementary Information, Table S1). For example, the ranges of ^{87}Sr/^{86}Sr, ^{143}Nd/^{144}Nd and ^{207}Pb/^{204}Pb ratios are 0.70723 to 0.70804, 0.51238 to 0.51250 and 15.591 to 15.622 for the Kyogatake volcano (Ryohaku area, #9, six samples) with the SiO_2 range from 49.5 to 66.8 wt%, and 0.70338 to 0.70359, 0.51289 to 0.51299 and 15.544 to 15.553 for the Kurofuji volcano (Fuji–Myoko area, #18, four samples) with the SiO_2 range from 51.4 to 59.0 wt%, respectively. The Nb/Pb ratio used in Fig. 3a is also almost independent of the silica content (see Supplementary Information, Table S1), and fractional crystallization hardly affects the ratio (see Supplementary Information, Methods). These pieces of evidence suggest that crustal contamination and/or differentiation are not the principal factor producing the wide compositional variations observed in central Japan, which is also supported by the assimilation, fractionation and crystallization modelling shown in Supplementary Information, Fig. S1a.

Received 25 September 2007; accepted 4 April 2008; published 11 May 2008.

References

1. Arculus, R. J. & Powell, R. Source component mixing in the regions of arc magma generation. *J. Geophys. Res.* **91**, 5913–5926 (1986).
2. Taylor, R. N. & Nesbitt, R. W. Isotopic characteristics of subduction fluids in an intra-oceanic setting, Izu-Bonin Arc, Japan. *Earth Planet. Sci. Lett.* **164**, 79–98 (1998).
3. Ishikawa, T. & Nakamura, E. Origin of the slab component in arc lavas from across-arc variation of B and Pb isotopes. *Nature* **370**, 205–208 (1994).
4. Moriguti, T., Shibata, T. & Nakamura, E. Lithium, boron and lead isotope and trace element systematics of Quaternary basaltic volcanic rocks in Northeastern Japan: Mineralogical controls on slab-derived fluid composition. *Chem. Geol.* **212**, 81–100 (2004).
5. Workman, R. K. & Hart, S. R. Major and trace element composition of the depleted MORB mantle (DMM). *Earth Planet. Sci. Lett.* **231**, 53–72 (2005).
6. Iwamori, H. Transportation of H_2O and melting in subduction zones. *Earth Planet. Sci. Lett.* **160**, 65–80 (1998).
7. Iwamori, H. Deep subduction of H_2O and deflection of volcanic chain towards backarc near triple junction due to lower temperature. *Earth Planet. Sci. Lett.* **181**, 41–46 (2000).
8. Hauff, F., Hoernle, K. & Schmidt, A. Sr–Nd–Pb composition of Mesozoic Pacific oceanic crust (Site 1149 and 801, ODP Leg 185): Implications for alteration of ocean crust and the input into the Izu-Bonin-Mariana subduction system. *Geochem. Geophys. Geosyst.* **4**, doi:10.1029/2002GC000421 (2003).

© 2008 Nature Publishing Group

9. Kelley, K. A., Plank, T., Ludden, J. & Staudigel, H. Composition of altered oceanic crust at ODP Sites 801 and 1149. *Geochem. Geophys. Geosyst.* **4**, doi:10.1029/2002GC000435 (2003).
10. Shimoda, G., Tatsumi, Y., Nohda, S., Ishizaka, K. & Jahn, B. M. Setouchi high-Mg andesites revisited: Geochemical evidence for melting of subducting sediments. *Earth Planet. Sci. Lett.* **160**, 479–492 (1998).
11. Hickey-Vargas, R. Isotope characteristics of submarine lavas from the Philippine Sea—Implications for the origin of arc and basin magmas of the Philippine tectonic plate. *Earth Planet. Sci. Lett.* **107**, 290–304 (1991).
12. Tatsumi, Y., Hamilton, D. L. & Nesbitt, R. W. Chemical characteristics of fluid phase released from a subducted lithosphere and origin of arc magmas—Evidence from high-pressure experiments and natural rocks. *J. Volcano. Geotherm. Res.* **29**, 293–309 (1986).
13. Aizawa, Y., Tatsumi, Y. & Yamada, H. Element transport by dehydration of subducted sediments: Implication for arc and ocean island magmatism. *Island Arc* **8**, 38–46 (1999).
14. Kogiso, T., Tatsumi, Y. & Nakano, S. Trace element transport during dehydration processes in the subducted oceanic crust.1. Experiments and implications for the origin of ocean island basalts. *Earth Planet. Sci. Lett.* **148**, 193–205 (1997).
15. You, C. F., Castillo, P. R., Gieskes, J. M., Chan, L. H. & Spivack, A. J. Trace element behavior in hydrothermal experiments: Implications for fluid processes at shallow depths in subduction zones. *Earth Planet. Sci. Lett.* **140**, 41–52 (1996).
16. Kawakatsu, H. & Watada, S. Seismic evidence for deep-water transportation in the mantle. *Science* **316**, 1468–1471 (2007).
17. Nakajima, J. & Hasegawa, A. Subduction of the Philippine Sea plate beneath southwestern Japan: Slab geometry and its relationship to arc magmatism. *J. Geophys. Res.* **112**, B08306 (2007).
18. Iidaka, T. *et al*. The upper boundary of the Philippine Sea plate beneath the western Kanto region estimated from S-P-converted wave. *Tectonophysics* **179**, 321–326 (1990).
19. Sekiguchi, S. A new configuration and an aseismic slab of the descending Philippine Sea plate revealed by seismic tomography. *Tectonophysics* **341**, 19–32 (2001).
20. Matsubara, M., Hayashi, H., Obara, K. & Kasahara, K. Low-velocity oceanic crust at the top of the Philippine Sea and Pacific plates beneath the Kanto region, Central Japan, imaged by seismic tomography. *J. Geophys. Res.* **110**, B12304 (2005).
21. Iwamori, H. & Zhao, D. Melting and seismic structure beneath the Northeast Japan Arc. *Geophys. Res. Lett.* **27**, 425–428 (2000).
22. Ono, S. Stability limits of hydrous minerals in sediment and mid-ocean ridge basalt compositions: Implications for water transport in subduction zones. *J. Geophys. Res.* **103**, 18253–18267 (1998).
23. Kawate, S. & Arima, M. Petrogenesis of the Tanzawa plutonic complex, central Japan: Exposed felsic middle crust of the Izu-Bonin-Mariana arc. *Island Arc* **7**, 342–345 (1998).
24. Seno, T. & Yamazaki, T. Low-frequency tremors, intraslab and interplate earthquakes in Southwest Japan—From a viewpoint of slab dehydration. *Geophys. Res. Lett.* **30**, doi:10.1029/2003GL018349 (2003).
25. Kersting, A. B., Arculus, R. J. & Gust, D. A. Lithospheric contributions to arc magmatism: Isotope variations along strike in volcanoes of Honshu, Japan. *Science* **272**, 1464–1468 (1996).
26. Knittel, U., Hegner, E., Bau, M. & Satir, M. Enrichment processes in the sub-arc mantle: A Sr–Nd–Pb isotopic and REE study of primitive arc basalts from the Philippines. *Can. Mineral.* **35**, 327–346 (1997).
27. Kobayashi, K. & Nakamura, E. Geochemical evolution of Akagi Volcano, NE Japan: Implications for interaction between island-arc magma and lower crust, and generation of isotopically various magmas. *J. Petrol.* **42**, 2303–2331 (2001).
28. Kimura, J.-I. & Yoshida, T. Contributions of slab fluid, mantle wedge and crust to the origin of Quaternary lavas in the NE Japan arc. *J. Petrol.* **47**, 2185–2232 (2006).
29. Kimura, J.-I. *et al*. Chemical diversity of the Ueno basalts, Central Japan: Identification of mantle and crustal contribution to arc basalts. *J. Petrol.* **43**, 1923–1946 (2002).

Supplementary Information accompanies this paper on www.nature.com/naturegeoscience.

Acknowledgements
We would like to thank T. Iidaka, T. Kaneko, Y. Kato, J.-I. Nakajima, I. Ogitsu and T. Seno for discussions and help, and R. King, T. Churikova for constructive comments.

Author contributions
H.N. carried out the field work and the chemical and isotopic analyses. H.N. and H.I. modelled mixing systematics of the isotopic and chemical compositions and J.-.I.K. conducted the laboratory work for isotopic analysis. All of the authors discussed the results and commented on the manuscript.

Author information
Reprints and permission information is available online at http://npg.nature.com/reprintsandpermissions. Correspondence and requests for materials should be addressed to H.N.

© 2008 Nature Publishing Group

CORRIGENDUM

Geochemical evidence for enhanced fluid flux due to overlapping subducting plates

HITOMI NAKAMURA, HIKARU IWAMORI AND JUN-ICHI KIMURA

Nature Geoscience **1,** 380–384 (2008)

In the Methods section and the Supplementary Information, the value of 207Pb/204Pb in altered oceanic basaltic crust for the Philippine Sea plate was incorrectly given as 15.629. The correct value is 15.4642. Also in the Methods section, the value of the sediment fluid/AOC fluid ratio for the Pacific plate fluid should have been given as 40:60, and on page 2 of the Supplementary Information, the value of dehydration from sediments at depths of greater than 30 km should have been given as 3.0 wt.%.

© 2008 Macmillan Publishers Limited. All rights reserved.

CORRIGENDUM

Geochemical evidence for enhanced fluid flux due to overlapping subducting plates

HITOMI NAKAMURA, HIKARU IWAMORI AND JUN-ICHI KIMURA

Nature Geoscience **1,** 380–384 (2008)

In the Methods section and the Supplementary Information, the value of 207Pb/204Pb in altered oceanic basaltic crust for the Philippine Sea plate was incorrectly given as 15.629. The correct value is 15.4642. Also in the Methods section, the value of the sediment fluid/AOC fluid ratio for the Pacific plate fluid should have been given as 40:60, and on page 2 of the Supplementary Information, the value of dehydration from sediments at depths of greater than 30 km should have been given as 3.0 wt.%.

© 2008 Macmillan Publishers Limited. All rights reserved.

Supplementary Information

Geochemical evidence for enhanced fluid flux due to overlapping subducting plates

Hitomi Nakamura, Hikaru Iwamori and Jun-Ichi Kimura

Supplementary Methods

Estimation of $^{207}Pb/^{204}Pb$ ratio of PHS-fluid

The PHS-fluid estimated from the rocks of Ryohaku Volcanoes could have been affected by PAC-fluid reducing $^{207}Pb/^{204}Pb$ of a 'true PHS-fluid', because the subducted PAC is also observed beneath Ryohaku Volcanoes (Fig.1). However, the observed maximum $^{207}Pb/^{204}Pb$ ratio (~15.65) of the subducting sediments and AOC is close to that of the estimated PHS-fluid (Fig.3b). Therefore, the estimated composition is thought to be close to that of 'true PHS-fluid'. The estimated composition is robust, even when Nb/Pb ratios of the data in Fig. 3a are corrected for fractional crystallization to estimate those of primary mantle melts, especially for plagioclase which has a relatively high partition coefficient for Pb (0.35)[30]: the $^{207}Pb/^{204}Pb$ ratio of PHS-fluid decreases by <0.01 % to 15.627 with maximum correction for 30 wt.% fractionation.

Estimation of multistage dehydration processes and compositions of the fluids

The results from numerical simulations[6,7], together with the studies on shallow dehydration processes[15], indicate that, for both PAC and PHS, (1) dehydration of 8-26 wt.% H_2O in sediment occurs at depth shallower than 30 km[15] (i.e., 10-30 wt.% H_2O contained in the pre-metamorphic bulk sediment before subduction decreases to 2-4 wt.% H_2O after the shallow dehydration), (2) dehydration of 1-3 wt.% H_2O contained in the subducting sediment that has undergone the process described in (1) produces 'sediment-fluid', while dehydration of 1-2 wt.% H_2O contained in the subducting AOC produces 'AOC-fluid', (3) these 'sediment-fluid' and 'AOC-fluid' migrate upwards to form a H_2O-saturated serpentinite layer just above the slab[6,16], which is thinner than the oceanic crust due to the mass balance of H_2O (e.g., 6.5 wt.% H_2O (the maximum H_2O content of serpentinite[6]) in the 1.6 km thick layer balances with 1.5 wt.% H_2O in the oceanic crust of 7 km thick), and (4) almost complete dehydration of this serpentinite layer at 150-300 km depth for PAC and 90-150 km for PHS.[6,7,16] Trace element and isotopic compositions of the

© 2008 Nature Publishing Group

sediment- and AOC-fluids are estimated based on those of initial materials (sediment and AOC sampled from the sea floors before subduction)[8-11] and mobilities of the elements[12-14]. The compositions of sediment-fluid (with the composition of initial sediment in brackets) are: 239 ppm (26.4 ppm) Pb, $^{207}Pb/^{204}Pb$=15.600, 487 ppm (164 ppm) Nd and $^{143}Nd/^{144}Nd$=0.51234 for PAC[8]; 326 ppm (36.1 ppm) Pb, $^{207}Pb/^{204}Pb$=15.629, 446 ppm (150 ppm) Nd and $^{143}Nd/^{144}Nd$=0.51233 for PHS[10], associated with 1.5 wt.% dehydration of the sediment at depths greater than 30 km. The compositions of AOC-fluid (with the composition of initial AOC in brackets) are: 24.7 ppm (0.436 ppm) Pb, $^{207}Pb/^{204}Pb$=15.4224, 243 ppm (11.4 ppm) Nd and $^{143}Nd/^{144}Nd$=0.51299 for PAC[9]; 37.8 ppm (0.669 ppm) Pb, $^{207}Pb/^{204}Pb$=15.629, 264 ppm (12.4 ppm) Nd and $^{143}Nd/^{144}Nd$=0.51310 for PHS[11], associated with 1.5 wt.% dehydration of AOC at depths greater than 30 km. These sediment-fluids and AOC-fluids react with the mantle wedge, which is assumed to be average-DMM[5] (0.02 ppm Pb, $^{207}Pb/^{204}Pb$=15.486, 0.52 ppm Nd, $^{143}Nd/^{144}Nd$=0.51313), just above the subducting slab to form serpentinite with 6.5 wt.% H_2O. This serpentinite breaks down as it subducts[6] to release PAC-fluid and PHS-fluid, which are almost identical in composition to the integrated sediment-fluid and AOC-fluid with the mixing proportion estimated above, since the concentrations of Nd and Pb in DMM are much lower than those in the fluids. Mobilities used in this calculation are: 0.988 and 0.65 during dehydration of sediment at shallower depths (< 30 km) and the deeper part (>30 km) for Pb, respectively, and 0.03 for Nd[13]; 0.846 for Pb and 0.309 for Nd in AOC[14]; 0.172 for Pb and 0.165 for Nd in serpentinite[12]. The PAC- and PHS-fluids ascend by porous flow, which is consistent with the time-scale of melt migration deduced from the U-Th secular disequilibria[31], to cause flux melting in the high-temperature part of the mantle wedge[7,21]. The chemical reaction (chromatographic effect) during the ascent is negligible since the elemental fluxes with fluids are much greater than those with mantle convection in the wedge.

Supplementary Figures

Figure S1 $^{87}Sr/^{86}Sr$ vs. $^{143}Nd/^{144}Nd$ and Nd/Pb vs. $^{207}Pb/^{204}Pb$ diagrams with the three mixing lines between PAC-fluid, PHS-fluid and DMM. a, $^{87}Sr/^{86}Sr$ vs. $^{143}Nd/^{144}Nd$ diagram. Symbols and data sources are the same as in Fig. 3b, except for the brown regions labeled "Hida Granite" (see AFC modeling below). The mixing model explains the Sr- and Nd-isotopic ratios of the volcanic

© 2008 Nature Publishing Group

rocks consistently with the $^{207}Pb/^{204}Pb$–$^{143}Nd/^{144}Nd$ systematics in Fig.3b. The consistency can be checked by the positions of four volcanoes (#2, #10, #23, #43) relative to the end-components, as well as the $^{87}Sr/^{86}Sr$ ratios calculated from R_{fluid} and α_{PHS} that are based on the independent $^{207}Pb/^{204}Pb$-$^{143}Nd/^{144}Nd$ systematics (see Table S2, columns 5 and 6). The results of AFC modeling are also shown as a light brown region enclosed by the solid brown lines. Hida Granite is exposed widely in Ryohaku Area and is well studied including its composition (dark brown region)[32,33]. For these reasons, it is selected as a representative candidate for the contaminant in the AFC modeling. Isotopic variation of volcanic rocks in Central Japan is significantly different from the possible range (light brown region) estimated by AFC modeling[34] with various combinations of assimilation-rate/crystallization-rate (r: 0.0-1.0), the melting degrees of contaminant (E: 0.0-1.0) and mantle (X: 0.01-0.2) and the melt fraction remaining in the system (F: 0.0-1.0). Compositions used in the AFC modeling are: 333 ppm Sr and 22.9 ppm Nd for Hida granite[33]. Partition coefficients used are: D_{Sr}=0.00019 (olivine), 0.002 (orthopyroxene) and 0.067 (clinopyroxene) for mafic melts, and 4.4 (plagioclase), 3.87 (alkalifelsper), 0.29 (biotite), 0.01 (amphibole) and 0.077 (opaque minerals) for felsic melts; D_{Nd}=0.008 (olivine), 0.0068 (orthopyroxene) and 0.21 (clinopyroxene) for mafic melts, and 0.19 (plagioclase), 0.025 (alkalifelsper), 0.339 (biotite), 1.6 (amphibole) and 0.03 (opaque minerals) for felsic melts[35-41]. We have also tested the other candidates for the contaminant (Funatsu Granite, Nohi Rhyolite) which widely expose in this area, and obtained the same conclusion that the AFC processes are not the major cause of the observed compositional variations of the Quaternary volcanic rocks in Central Japan. **b,** Nd/Pb vs. $^{207}Pb/^{204}Pb$ diagram. Symbols and data sources are the same as in Fig. 3b. The mixing model explains the observed data in Central Japan. Although the numerical studies suggest that the subducted PAC and PHS slabs beneath Central Japan is too cold to induce slab melting[6,7], melts derived from sediments (sediment-melt) and AOCs (AOC-melt) during partial melting of the subducting PAC and PHS slabs have been also tested for comparison. Such melts are calculated as the mixtures of sediment-melt plus AOC-melt (large symbol 'X') or sediment-melt plus AOC-fluid (large symbol '+') to satisfy the $^{207}Pb/^{204}Pb$ constraints as in Fig.3b. The 1% batch melting of AOC leaving garnet amphibolite residuum (30% clinopyroxene, 30% garnet and 40% amphibole) and the corresponding partition coefficients are assumed[42]. The 75% batch melting of sediment leaving restite composed of 40% garnet, 40% quartz, and 20%

© 2008 Nature Publishing Group

sillimanite and the corresponding partition coefficients are assumed[43]. The results show that Nd/Pb ratios of the slab-derived melts are too high to explain most of the observed variation, suggesting that the slab dehydration is likely to produce aqueous fluid, rather than melt. However, the possibility of slab melting and its contribution to PHS-fluid cannot be entirely ruled out, since some of the data with high $^{207}Pb/^{204}Pb$ and Nd/Pb ratios may be explained by involvement of such a melt component, especially a sediment-derived melt from the PHS slab (orange triangle, 'X' and '+'), as well as the sediment-derived aqueous fluid (orange star).

Figure S2 Pb-isotopic systematics with the three mixing lines between PAC-fluid, PHS-fluid and DMM. a, $^{207}Pb/^{204}Pb$ vs. $^{208}Pb/^{204}Pb$ diagram. **b,** $^{207}Pb/^{204}Pb$ vs. $^{206}Pb/^{204}Pb$ diagram. Symbols and data sources are the same as in Fig. 3b. The mixing model explains the three Pb-isotopic ratios of the volcanic rocks in Central Japan consistently with the $^{207}Pb/^{204}Pb$–$^{143}Nd/^{144}Nd$ systematics in Fig.3b. The consistency can be checked by the positions of four volcanoes (#2, #10, #23 and #43) relative to the end-components. Both diagrams show a linear correlation between the three Pb-isotopic ratios of the volcanic rocks in Central Japan, indicating that they can be represented by one of the Pb-isotopic ratios. However, Fig.S2b shows that the $^{206}Pb/^{204}Pb$ ratios of the end-components overlap with each other, and cannot resolve R_{fluid} and α_{PHS}.

Supplementary Tables

Table S1 Chemical and isotopic compositions of the Quaternary volcanic rocks in Central Japan. Isotopic compositions of 46 samples were determined at Shimane University using the thermal ionization mass spectrometer MAT262 (TIMS) for Nd, and the multiple collector-inductively coupled plasma mass spectrometry (MC-ICP-MS) for Sr and Pb. Replicate analyses of La Jolla Nd standard (n=10) and NIST SRM981 Pb (n=75) gave mean values with 2σ (standard deviation) as follows: $^{143}Nd/^{144}Nd = 0.511840 \pm 0.000017$ and $^{207}Pb/^{204}Pb = 15.4921 \pm 0.0047$. The uncertainties of individual analysis is represented by 2SD (2 standard deviations) in the table. The SiO_2 and trace element abundances were measured with the X-ray fluorescence spectrometer (PhilipsPW-1480 XRF) and the inductively coupled plasma mass spectrometer (Agilent 7500c ICP-MS) at the University of Tokyo. The analytical uncertainties

© 2008 Nature Publishing Group

(1σ) of SiO_2, Sr, Nd, Pb and Nb are 0.16 wt.%, 0.41 ppm, 1.2 ppm, 1.0 ppm and 0.17 ppm, respectively.

Table S2 Calculated amounts of fluid added to the mantle wedge (R_{fluid}) and the proportion of PAC-fluid and PHS-fluid (α_{PHS}). R_{fluid} and α_{PHS} for each volcano are calculated based on the Pb-Nd isotopic systematics shown in Fig.3b. In order to test the consistency of the estimates, the Sr isotopic ratios are calculated ('Calculated $^{87}Sr/^{86}Sr$' in the 5th column) from the obtained parameters (R_{fluid} and α_{PHS}) and the compositions of DMM, PAC-fluid and PHS-fluid. The differences from the observed values ($\Delta(^{87}Sr/^{86}Sr) = |(^{87}Sr/^{86}Sr)_{observation}-(^{87}Sr/^{86}Sr)_{calculated}|$) are also shown in the 6th column, indicating that the isotopic variations of Pb, Nd and Sr are consistently explained by the mixing model.

Supplementary References

30. Ewart, A. & Griffin, W.L. Application of proton-microprobe data to trace-element partitioning in volcanic rocks. *Chem. Geol.* **117**, 251-284 (1994)

31. Hawkesworth, C.J., Turner, S.P., McDermott, F., Peate, D.W. & Calsteren P. U-Th isotopes in arc magmas: Implications for element transfer from the subducted crust. *Science* **276**, 551-555 (1997)

32. Tanaka, S. & Kagami, H. The origin of early Mesozoic granitoid exposed in Hida Zone – A study from Nd-Sr isotopic compositions. *Chikyu* **12**, 391-395 (1990)

33. Tanaka, S. & Ohtsubo, T. Trace element in the Funatsu granitic rocks - with special reference to high Sr contents in the Hayatsukigawa intrusion. *Chikyu Kagaku* **41**, 101-113 (1987)

34. Depaolo, D.J. A neodymium and strontium isotopic study of the Mesozoic calc-alkaline granitic batholiths of the Sierra-Nevada and Peninsular Ranges, California. *J. Geophys. Res.* **86**, 470-488 (1981)

35. McKenzie, D. & Onions, R.K. Partial melt distributions from inversion of rare-earth element concentrations. *J. Petrol.* **32**, 1021-1091 (1991)

36. Paster, T.P., Schauwec, D.S. & Haskin, L.A. Behavior of some trace-elements during solidification of Skaergaard layered series. *Geochim. Cosmochim. Acta* **38**, 1549-1577 (1974)

37. Kelemen, P.B., Shimizu, N. & Dunn, T. Relative depletion of niobium in some

© 2008 Nature Publishing Group

arc magmas and the continental-crust - Partitioning of K, Nb, La and Ce during melt/rock reaction in the upper-mantle. *Earth Planet. Sci. Lett.* **120**, 111-134 (1993)
38. Nash, W.P. & Crecraft, H.R. Partition-coefficients for trace-elements in silicic magmas. *Geochim. Cosmochim. Acta* **49**, 2309-2322 (1985)
39. Bacon, C.R. & Druitt, T.H. Compositional evolution of the zoned calcalkaline magma chamber of Mount-Mazama, Crater Lake, Oregon. *Contrib. Mineral. Petrol.* **98**, 224-256 (1988)
40. Ewart, A. & Griffin, W.L. Application of proton-microprobe data to trace-element partitioning in volcanic-rocks. *Chem. Geol.* **117**, 251-284 (1994)
41. Sisson, T.W. Pyroxene-high silica rhyolite trace-element partition-coefficients measured by ion microprobe. *Geochim. Cosmochim. Acta* **55**, 1575-1585 (1991)
42. Gomez-Tuena, A., Langmuir, C.H., Goldstein, S.L., Straub, S.M. & Ortega-Gutiérrez, F. Geochemical evidence for slab melting in the Trans-Mexican volcanic belt *J. Petrol.* **48**, 537-562 (2007)
43. Tatsumi, Y. Geochemical modeling of partial melting of subducting sediments and subsequent melt-mantle interaction: Generation of high-Mg andesites in the Setouchi volcanic belt, Southwest Japan. *Geology* **29**, 323-326 (2001)

© 2008 **Nature Publishing Group**

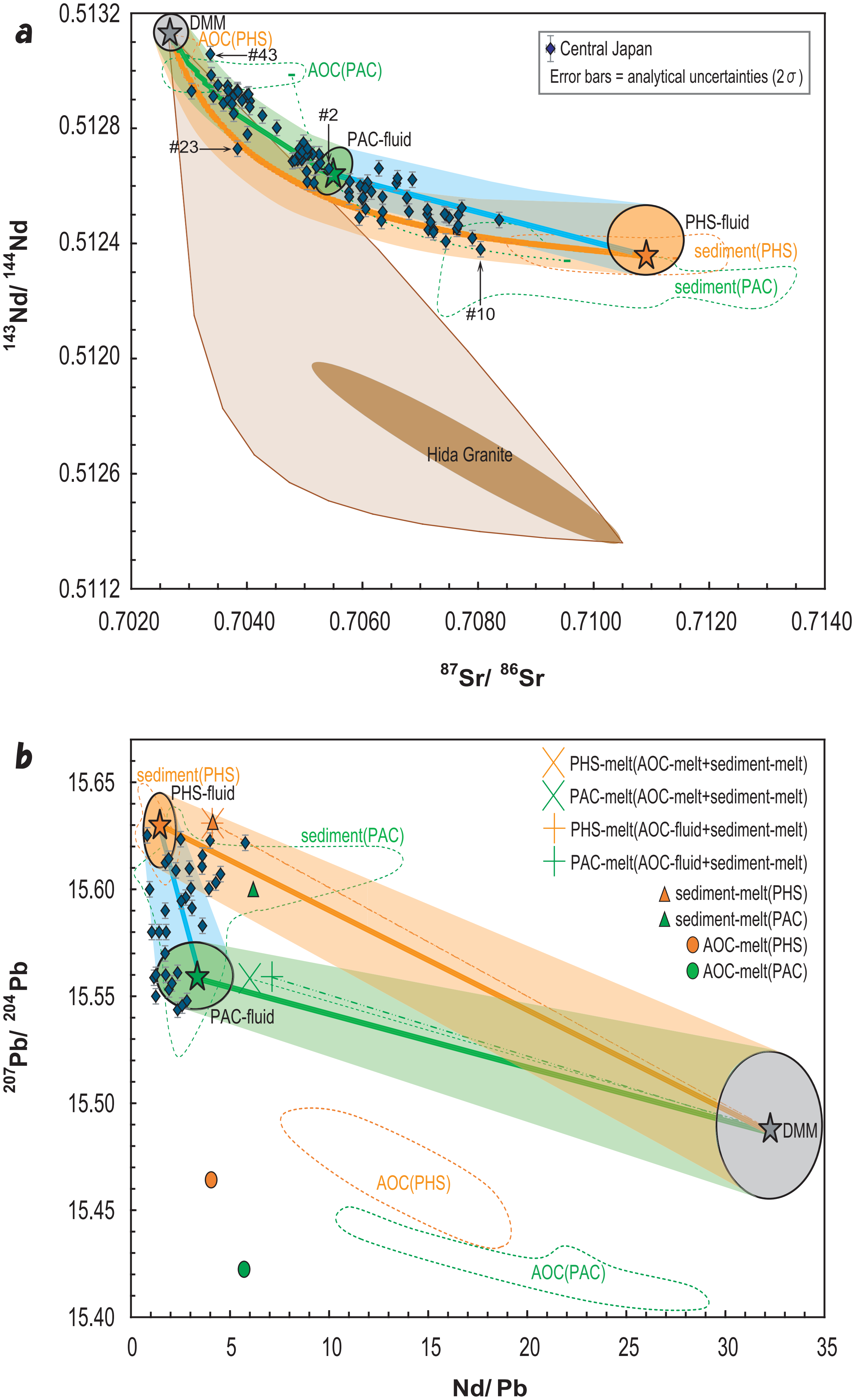

NGS-2007-09-00239A

© 2008 Nature Publishing Group

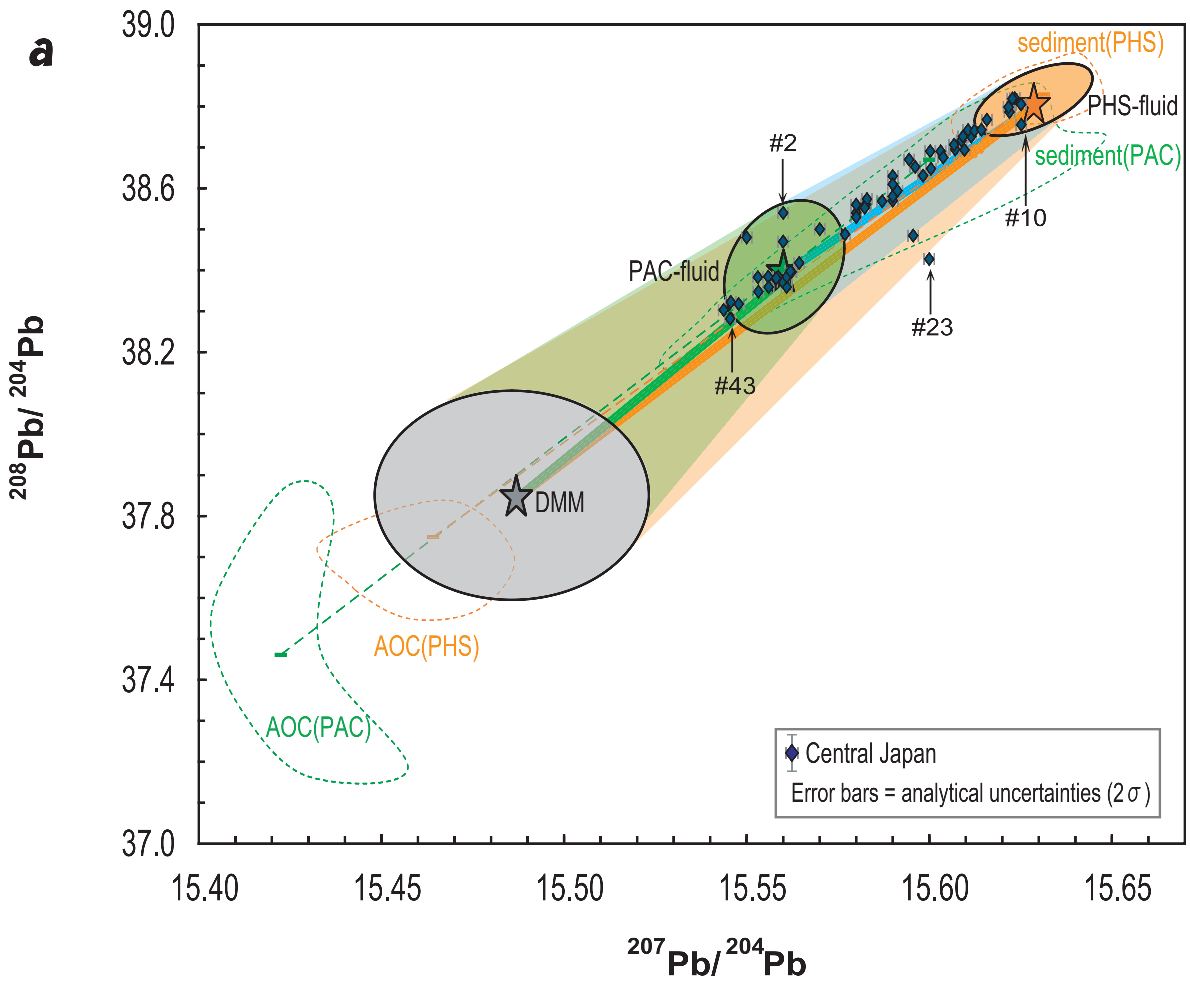

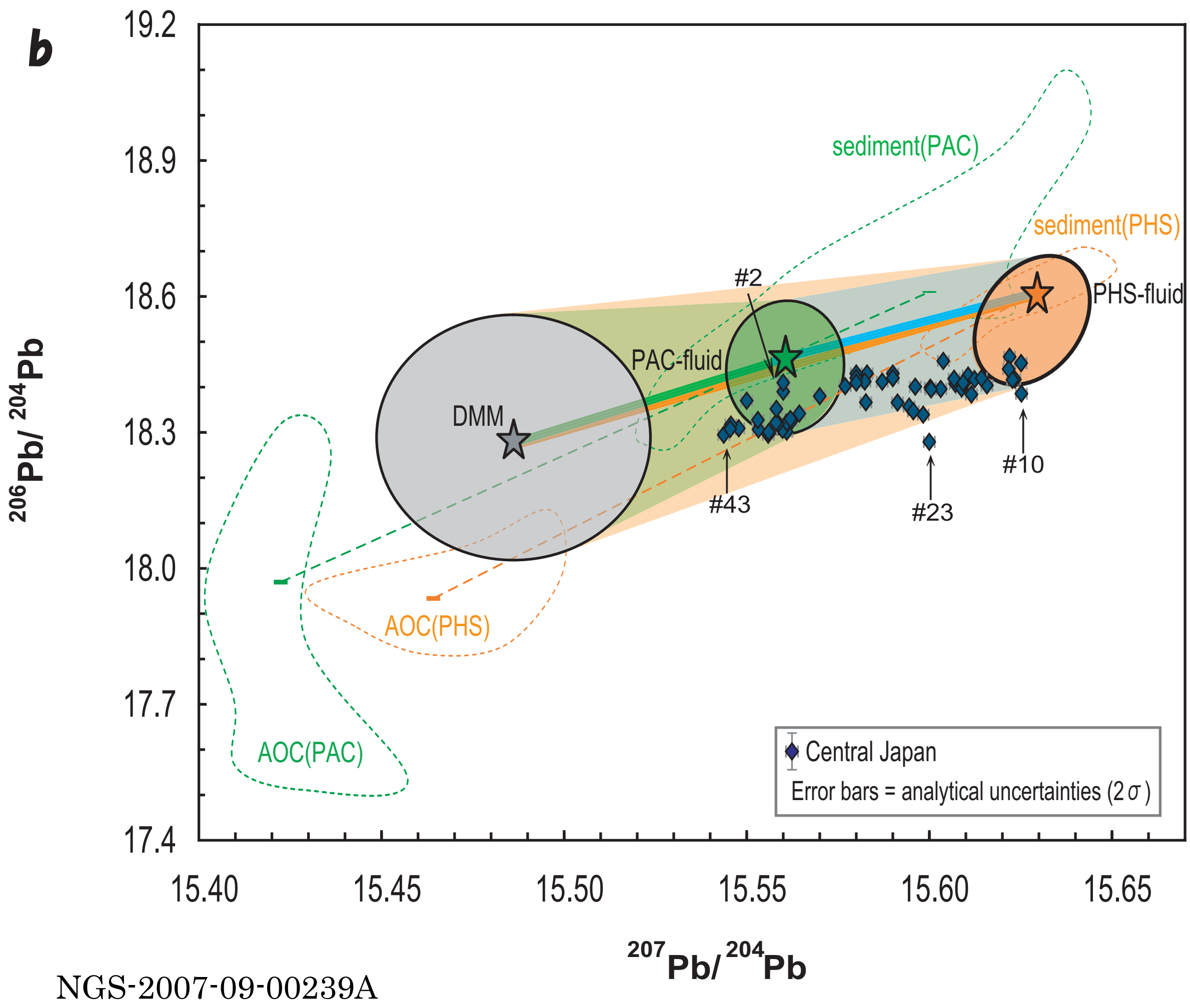

NGS-2007-09-00239A

© 2008 Nature Publishing Group

ID no.	Volcano	SiO_2 (wt. %)	$^{87}Sr/^{86}Sr$	2SD	$^{143}Nd/^{144}Nd$	2SD	$^{206}Pb/^{204}Pb$	2SD	$^{207}Pb/^{204}Pb$	2SD	$^{208}Pb/^{204}Pb$	2SD	Sr (ppm)	Nd (ppm)	Pb (ppm)	Nb (ppm)
5	Kenashi	55.99	0.704055	1.45E-05	0.512895	1.07E-05	18.342	0.0014	15.564	0.0012	38.418	0.0032	287.70		3.95	0.28
5	Kenashi	57.06	0.704030	1.30E-05	0.512918	8.97E-06	18.330	0.0015	15.562	0.0013	38.398	0.0035	279.69		6.46	1.29
5	Kenashi	62.35	0.704001	1.47E-05	0.512915	9.17E-06	18.322	0.0013	15.558	0.0011	38.379	0.0028	291.14		6.49	0.47
7	Dainichigatake	60.98	0.707121	1.39E-05	0.512501	1.50E-05	18.397	0.0014	15.609	0.0013	38.717	0.0037	505.49	22.24	9.81	9.24
7	Dainichigatake	57.56	0.707125	1.44E-05	0.512518	1.47E-05	18.396	0.0019	15.603	0.0017	38.690	0.0047	701.56	25.35	5.92	7.48
7	Dainichigatake	54.51	0.706587	1.20E-05	0.512609	1.05E-05	18.395	0.0017	15.600	0.0014	38.648	0.0036	670.78	24.97	8.26	7.34
9	Kyogatake	66.80	0.707500	1.33E-05	0.512490	1.08E-05	18.409	0.0011	15.610	0.0013	38.694	0.0034	486.75	34.51	11.71	9.19
9	Kyogatake	61.43	0.707448	1.22E-05	0.512499	1.12E-05	18.418	0.0018	15.607	0.0018	38.706	0.0049	610.75		6.49	8.07
9	Kyogatake	56.79	0.707633	1.43E-05	0.512451	1.05E-05	18.467	0.0017	15.622	0.0016	38.786	0.0048	630.11		9.90	8.15
9	Kyogatake	55.97	0.707228	1.40E-05	0.512439	1.10E-05	18.410	0.0011	15.609	0.0011	38.727	0.0033	652.59		10.87	5.62
9	Kyogatake	49.52	0.707659	1.31E-05	0.512462	1.10E-05	18.440	0.0021	15.622	0.0019	38.798	0.0049	714.83	19.00	3.29	3.93
9	Kyogatake	57.79	0.707422	9.50E-06	0.512502	1.09E-05	18.425	0.0007	15.611	0.0008	38.742	0.0023	574.68	27.80	7.75	8.31
9	Kyogatake	51.11	0.708043	1.36E-05	0.512380	1.10E-05	18.366	0.0014	15.591	0.0012	38.594	0.0032	683.02	18.14	5.89	2.53
10	Eboshiwashigatake	60.31	0.707140	1.42E-05	0.512447	1.04E-05	18.417	0.0013	15.623	0.0012	38.820	0.0032	544.51	27.41	10.93	8.02
10	Eboshiwashigatake	57.78	0.707180	1.45E-05	0.512473	9.50E-06	18.404	0.0011	15.616	0.0009	38.768	0.0025	560.40	33.47	9.28	7.86
10	Eboshiwashigatake	56.67	0.707230	1.33E-05	0.512448	1.05E-05	18.416	0.0010	15.623	0.0009	38.819	0.0026	622.25	27.01	6.76	6.46
10	Eboshiwashigatake	63.06	0.707443	1.44E-05	0.512407	1.06E-05	18.386	0.0034	15.625	0.0029	38.755	0.0073	531.84	25.09	30.67	7.44
11	Dainichiyama	64.49	0.707662	1.20E-05	0.512499	1.08E-05	18.417	0.0010	15.612	0.0012	38.740	0.0039	638.90	28.33	16.29	11.56
11	Dainichiyama	61.73	0.707901	1.35E-05	0.512418	1.03E-05	18.419	0.0012	15.614	0.0014	38.743	0.0050	643.22	22.57	11.86	8.65
12	Hakusan	61.51	0.706804	1.40E-05	0.512511	1.05E-05	18.357	0.0014	15.594	0.0013	38.670	0.0037	640.30	19.07	7.51	5.71
12	Hakusan	51.68	0.703838	1.37E-05	0.512729	1.11E-05	18.306	0.0034	15.560	0.0030	38.373	0.0074	654.63		10.79	4.56
13	Ontake	53.02	0.705207	1.42E-05	0.512666	1.01E-05	18.407	0.0024	15.607	0.0020	38.695	0.0056	778.94	27.12	6.00	6.24
13	Ontake	53.43	0.704933	1.37E-05	0.512699	1.14E-05	18.384	0.0015	15.612	0.0012	38.727	0.0029	646.33		6.34	5.77
13	Ontake	50.79	0.704981	1.45E-05	0.512733	1.06E-05	18.366	0.0024	15.583	0.0021	38.561	0.0053	653.42		4.56	5.78
14	Myoko	50.15	0.704518	1.46E-05	0.512802	1.15E-05	18.402	0.0014	15.577	0.0017	38.488	0.0076	427.67		5.13	1.33
14	Myoko	55.82	0.703772	1.33E-04	0.512851	1.17E-05	18.295	0.0012	15.556	0.0013	38.384	0.0041	329.64		6.19	2.05
14	Myoko	59.89	0.704268	1.42E-05	0.512845	1.07E-05	18.327	0.0016	15.553	0.0016	38.383	0.0061	314.22		6.66	2.25
16	Shirouma-oike	*54.21*	*0.706088*		*0.512611*		18.430	0.0013	15.583	0.0011	38.574	0.0029				4.62
18	Kurofuji	56.64	0.703419	1.33E-05	0.512911	1.04E-05	18.295	0.0035	15.544	0.0030	38.303	0.0074	818.63	12.64	5.37	2.26
18	Kurofuji	51.40	0.703382	1.44E-05	0.512985	1.42E-05	18.309	0.0015	15.548	0.0013	38.317	0.0040	1004.05	13.58	4.81	1.96
18	Kurofuji	53.69	0.703501	1.45E-05	0.512950	1.08E-05	18.317	0.0015	15.546	0.0014	38.322	0.0044	743.70	10.49	4.06	1.80
18	Kurofuji	59.02	0.703593	1.47E-05	0.512887	1.10E-05	18.307	0.0011	15.553	0.0011	38.348	0.0033	710.39	11.39	5.94	2.17
20	Tateyama	*51.78*	*0.706155*		*0.512580*		18.399	0.0015	15.600	0.0018	38.690	0.0064				8.48
20	Tateyama	*60.43*	*0.705995*		*0.512554*		18.401	0.0029	15.596	0.0025	38.652	0.0071				7.14
21	Nomugitoge	*58.77*	0.706769	1.39E-05	0.512558	1.07E-05	18.453	0.0012	15.625	0.0012	38.805	0.0044				9.80
23	Asama	61.31	0.704046	1.37E-05	0.512874	1.22E-05	18.279	0.0014	15.600	0.0013	38.427	0.0034	322.12	7.55	8.04	2.70
36	Omeshi	59.44	0.703680	1.45E-05	0.512901	1.05E-05	18.322	0.0016	15.561	0.0014	38.384	0.0037	405.90	13.66	5.81	1.78
36	Omeshi	62.94	0.703917	1.43E-05	0.512897	1.05E-05	18.320	0.0011	15.559	0.0012	38.384	0.0035	278.25	11.35	9.78	1.60
37	Tomuro	54.15	0.704011	1.45E-05	0.512779	9.55E-06	18.301	0.0012	15.556	0.0012	38.359	0.0025	548.57	23.70	11.45	5.28
40	Azumaya	64.62	0.703758	1.28E-05	0.512908	1.00E-05	18.325	0.0013	15.562	0.0011	38.396	0.0028	322.26		7.66	2.36
40	Azumaya	55.16	0.703829	1.45E-05	0.512928	1.10E-05	18.302	0.0015	15.561	0.0016	38.359	0.0039	406.65		5.27	0.86
41	Takahara	54.50	0.705961	1.30E-05	0.512600	1.01E-05	18.412	0.0020	15.587	0.0012	38.569	0.0032	261.11		6.65	1.91
41	Takahara	61.98	0.706284	1.32E-05	0.512661	1.09E-05	18.412	0.0036	15.582	0.0035	38.552	0.0082	230.63		6.43	1.78
41	Takahara	54.73	0.705047	1.38E-05	0.512614	1.02E-05	18.346	0.0022	15.596	0.0017	38.484	0.0042	304.08		5.44	1.21
42	Nishimochiya	46.47	0.703042	1.26E-05	0.512929	1.13E-05	18.352	0.0019	15.558	0.0016	38.381	0.0052	568.45		10.61	1.57
43	Fuji (Komitake)	48.98	0.703368	1.47E-05	0.513058	9.32E-06	18.308	0.0017	15.545	0.0013	38.282	0.0039	455.81		5.59	1.72

itallic: unpublished data from Kimura (2002)

NGS-2007-09-00239A

© 2008 **Nature Publishing Group**

ID no.	Volcano	α_{PHS} (weight ratio)	R_{fluid} (kg fluid / kg mantle)	Calculated $^{87}Sr/^{86}Sr$	$\Delta(^{87}Sr/^{86}Sr)$
1	Nekoma	0.10	0.010	0.705216	0.00031
2	Akagi	0.12	0.025	0.706144	0.00011
5	Kenashi	0.08	0.007	0.704795	0.00074
7	Dainichigatake	0.52	0.040	0.707497	0.00091
9	Kyogatake	0.85	0.030	0.708161	0.00050
10	Eboshiwashigatake	0.90	0.040	0.708677	0.00145
11	Dainichiyama	0.60	0.020	0.706963	0.00094
12	Hakusan	0.30	0.018	0.706197	0.00236
13	Ontake	0.68	0.006	0.705272	0.00007
14	Myoko	0.17	0.005	0.704506	0.00001
15	Ueno	0.10	0.003	0.703927	0.00117
16	Shirouma-oike	0.17	0.020	0.706049	0.00004
18	Kurofuji	0.01	0.003	0.703874	0.00049
20	Tateyama	0.40	0.020	0.706518	0.00036
21	Nomugi-toge	0.95	0.015	0.707334	0.00057
23	Asama	0.60	0.002	0.703802	0.00024
26	Nasu	0.15	0.020	0.706010	0.00152
28	Nantai	0.23	0.014	0.705791	0.00022
36	Omeshi	0.06	0.003	0.703904	0.00022
37	Tomuro	0.00	0.008	0.704847	0.00084
40	Azumaya	0.08	0.007	0.704795	0.00097
41	Takahara	0.40	0.010	0.705650	0.00031
42	Nishimotiya	0.05	0.002	0.703740	0.00070
43	Fuji	0.10	0.001	0.703019	0.00035
46	Nyoho	0.15	0.013	0.705577	0.00020

NGS-2007-09-00239A

© 2008 Nature Publishing Group